Meshless Elasticity Model and Contact Mechanics-based Verification Technique

Rifat Aras[1], Yuzhong Shen[1], Michel Audette[1], Stephane Bordas[2]

[1]Department of Modeling, Simulation, and Visualization Engineering, Old Dominion University, Norfolk, VA, United States

[2]Institute of Mechanics and Advanced Materials, Cardiff University, Wales, UK

Abstract Mesh-based techniques are well studied and established methods for solving continuum biomechanics problems. When the problem at hand involves extreme deformations or artificial discontinuities, meshless methods provide several advantages over the mesh-based methods. This work discusses the Moving Least Square approximation-based meshless collocation method for simulating deformable objects and presents a verification technique that is based on the Hertzian theory of non-adhesive elastic contact. The effectiveness of the Hertzian contact theory as a means for verification was first tested and proven through a well-established FEM code, FEBio. The meshless method was implemented as a reusable component for the SOFA framework, an open source software library for real-time simulations. Through experimentation, the Hertzian theory has been tested against SOFA hexahedral FEM and the meshless models within the SOFA framework. Convergence studies and L2 error curves are provided for both models. Experimental results demonstrated the effectiveness of the implementation of the meshless method.

1 Introduction

Soft tissue models have a wide range of application areas with particular focus on real-time medical simulations. As a result, accurate interactive modeling of soft tissue is an important and well-established research field in continuum biomechanics studies.

A continuum model typically relies on an underlying mesh structure either in 2D or 3D depending on the nature and the requirements of the problem. A breadth-first classification of mesh-based continuum models includes mass-spring networks [1], Finite Element Methods [2], Finite Volume Methods [3], and Finite Difference Methods [4].

Originally developed for molecular dynamics problems and astrophysical simulations, meshless (mesh-free) methods offer an appealing alternative to mesh-based methods when the problem involves large deformations and imposed dis-

continuities such as cracks and cuts. In this work, the meshless method is implemented as a component under the open-source SOFA library, which focuses on real-time interactive simulations with an emphasis on medical simulations. In conjunction with the interactive simulation requirement, we assume the linear property of the soft tissue model within a specific range of the strain-stress curve. This assumption is parallel with the small strain and linear material assumptions of the Hertzian contact theory.

There have been numerous approaches to modeling mechanics of soft tissues. Among those is the early work of Sederberg and Parry [5] that presented a technique for deforming solid geometric models in an intuitive free-form manner. The deformations were based on interpolating trivariate Bernstein polynomials, and could be applied either globally or locally with volume preservation. Free-form deformation is an approximate and simple method for deforming solid objects; however the lack of physical basis is grounds for excluding it as an option for realistic medical simulations. The work of Frisken-Gibson [6] modified the traditional voxel based representation of volumetric objects and presented a linked volume representation that was capable of handling interactive object manipulations such as carving, cutting, tearing, and joining, but still unable to produce physically realistic results. An alternative to volumetric methods is to use mass-spring models [7] and membrane based approximations that utilize spring meshes [8]. A spring mesh is composed of vertices and edges, in which each edge is realized as a spring that connects vertices pair-wise, and each vertex is idealized as a point mass. Although spring meshes employ physical equations like Hooke's law, it is difficult to reproduce specific elastic material properties even with very careful distribution of spring stiffness through the mesh and suffer from poor numerical stability.

The early work of Bro-Nielsen discussed a fast adaptation of finite element modeling to satisfy speed and robustness requirements in a surgical simulation setting [9]. In this work, the body part was modeled as a 3D linear elastic solid that consisted of particles, which were deformed into a new shape when forces were applied to the elastic solid. The author incorporated a technique called condensation in order to achieve interactive simulation. In the finite element modeling context, condensation translates into obtaining a more compact version of the system model by rearranging the terms of the matrix equations. In this work, the author condensed the equations by only considering the finite element nodes on the surface of the model.

A number of recent techniques have addressed the fidelity versus efficiency trade-off. Another important work in the area is the finite element model based on Total Lagrangian Explicit Dynamics (TLED) by Miller et al. [10]. The difference between the TLED based finite element model and other approaches is using the original reference configuration of the object to calculate the stress and strain tensors during a simulation step. As a result of expressing computations in the reference coordinates, the authors were able to pre-compute spatial derivatives. The pre-computation of the spatial derivatives leads to efficiency in terms of computational resources, while being capable of handling geometric and material non-

linearities. In their work, the authors employed the central difference based explicit integration rather than the implicit integration scheme. With this choice, they were able to avoid solving the set of non-linear algebraic equations that are required by the implicit integration at each time step. However, the use of explicit integration brings limitation on the time step size. The authors justified their implementation choice by stating that the relatively lower stiffness (Young's modulus) value of the soft tissue relaxes the time step limitation considerably compared to the typical simulations involving more stiff material like steel or concrete.

Another attempt to increase the computational efficiency of the elastic model in the context of interactive simulation was discussed in the work of Marchesseau et al. [11]. The authors presented a new discretization method called Multiplicative Jacobian Energy Decomposition (MJED), which allows the simulation to assemble the stiffness matrix of the system faster than the traditional Galerkin FEM formulation. The authors reported up to five times faster computations for the St. Venant Kirchoff materials. For validation purposes, the authors compared the MJED approach to the traditional FEM implementation in the SOFA framework [12], referred to as the *standard FEM* implementation.

FEM techniques have dominated the field of computational mechanics in the past several decades. They have been widely used for modeling physical phenomena such as elasticity, heat transfer, and electromagnetism and they heavily rely on the assumption of a continuous domain. When the problem domain no longer complies with this continuum assumption, the rationale behind using an FEM based solution disappears. FEM is also not well suited to problems involving extreme mesh distortions that result in degenerate element shapes, moving discontinuities that do not align with the element edges such as propagating cracks, and advanced material transformations such as melting of a solid or freezing. To address these issues, significant interest has been developed towards a different class of methods for solving PDEs, namely meshless or mesh-free methods [13, 14]. The very first meshless method dated back to 1977 [15] and proposed a smoothed particle hydrodynamics (SPH) method that was used to model theoretical astrophysical phenomena such as galaxy formation, star formation, stellar collisions, and dust clouds. Its meshless Lagrangian nature allowed diverse usage areas besides astrophysics such as fluid flow, ballistics, volcanology, and oceanography [16].

Although the SPH method eliminates the necessity of a mesh structure and allows the solution of unbounded problems, it also has its limitations. Because of its simplistic kernel based approximation scheme, it fails to reproduce even first order polynomials, resulting in severe consistency problems [13]. To alleviate this problem, methods that utilize moving least squares (MLS) approximations have been developed. The first work that used MLS approximations in a Galerkin method is the work of Nayroles et al. [17], which was refined by Belytschko et al. [18] and named Element-Free Galerkin (EFG) method. This class of methods, different from the SPH method, use shape functions in approximations that are essentially corrected versions of compact supported weight functions. The shape functions

are obtained by first representing the approximation as a product of a polynomial basis and a vector of unknown coefficients. Then, a functional is created by taking the weighted sum of square of the approximation error. By taking the derivative of this functional with respect to the unknown coefficients and setting it to zero for minimizing the approximation error, we obtain a set of equations that are reorganized to solve for the MLS shape functions. The order of consistency of the MLS approximation scheme depends on the order and completeness of the used basis function. If the basis function used in the approximation is a complete polynomial of order k, then the MLS approximation is said to be k^{th} order consistent. This fact makes the MLS based approximations more consistent than the SPH method.

Another technique that has used the MLS approximation is the work of Mueller et al. [19] and forms the basis of the meshless method discussed in this paper. In this work, the authors calculated the spatial derivatives of the deformation gradient only at the particle locations similar to the meshless collocation methods. This technique is capable of simulating a wide range of material properties from very stiff materials to soft ones and also handles plastic deformations as well.

Horton et al. [20] proposed a new kind of meshless method named meshless total Lagrangian explicit dynamics method. In this work, the authors extended their previous TLED algorithm [10] to the meshless discretization methodology by precomputing the strain-displacement matrices. Their method is a fully explicit method, meaning not requiring implicit time integration and costly solution of large system of equations. Different than our nodal integration approach, their proposed algorithm integrates over a regular background grid with single integration point per cell.

In this work, we present the details of the MLS approximation-based meshless collocation method for soft-tissue deformation. Specific contributions are SOFA implementation of the presented meshless method, a new verification technique with the Hertzian non-adhesive contact theory, and verification of the algorithm with well-established FEM code and our SOFA component that implements the presented meshless method.

The rest of the paper is organized as follows. Section 2 describes the details of the meshless elasticity algorithm, including node distribution, construction of support domains, used weight function, and calculation of nodal simulation values such as mass, volume, and density. Operations involved in the MLS approximation of the deformation gradient are discussed, followed by the internal elastic force calculation procedure. Section 3 describes the implementation details of the presented meshless method in SOFA and presents the verification techniques for the elasticity model along with the virtual experiment setup and the results. Section 4 concludes the paper and discusses possible future extensions to the presented work.

2 Algorithm

2.1 Discretization of the Continuum

Node distribution is the first step in the presented meshless collocation algorithm, which supports both regular and hierarchical distribution of the nodes through the simulation domain. In the case of a simulation domain with a regular geometric shape, regular distribution of the nodes is the natural choice. On the other hand, if the simulation domain has a complex geometry, the regular distribution simply becomes inapplicable. In this case, we sample the volumetric simulation domain bounded by the complex boundary surface by hierarchically sampling the volume. In the work of Pauly et al.[21], the authors used a balanced octree data structure to distribute the nodes inside the volume. In this work, we first tetrahedralize the simulation domain with well-established computational geometry libraries like TetGen [22] and CGAL [23] and then use the set of vertices of the tetrahedra as the meshless node locations. In this way, similar to graded finite element meshing techniques, we can have higher node density close to the domain boundary and fewer nodes towards the interior of the volume where the material is continuous.

Meshless methods represent a deformable body by a cloud of particles with overlapping support domains. Quantities such as mass, volume, support size, strain, and stress are stored and updated per particle for the duration of the simulation. In this work, the support domains of the particles are spherical and their radii are computed by finding the average distance of the central node to its *k*-nearest neighbors. For efficient neighborhood search purposes, a *k*-d tree data structure is used.

Weight (kernel) function in the meshless method context is an element that describes the way meshless nodes affect each other and how the material values of the continuum such as mass, volume, and density are distributed among the nodes. The neighboring particles that fall inside the support domain of a central particle are weighted using the polynomial kernel function

$$w(r_{ij}) = \begin{cases} 1 - 3r_{ij}^2 + 3r_{ij}^4 - r_{ij}^6, & r_{ij} \le 1 \\ 0, & r_{ij} > 1 \end{cases} \tag{1}$$

with $r_{ij} = \dfrac{\left\| \mathbf{x}_j - \mathbf{x}_i \right\|}{h_i}$, where $\mathbf{x}_i$ and $\mathbf{x}_j$ are the current locations of the neighboring and central particles, respectively and h_i is the support radius of the central particle *i*.

The mass and density of a meshless node are assigned at the beginning and kept fixed throughout the simulation. The mass values are initialized with

$$m_i = s\bar{r}_i^3 \rho\,, \tag{2}$$

where ρ is the material density value, $\bar{r}_i$ is the average distance of the i^{th} node to its *k*-nearest neighbors, and s is a scaling factor that is chosen so that the average of the assigned densities is close to the actual material density. The assigned mass value of a meshless node is spread around the node with the kernel function. Therefore the density of a meshless node is calculated after the mass allocation step by taking the weighted average of the masses of the neighboring nodes

$$\rho_i = \sum_j m_j w(r_{ij}) \tag{3}$$

In this work, spatial integration is performed through the nodal integration technique. Compared to other spatial integration techniques that utilize a background mesh or grid with multiple integration points per region, nodal integration is fast and efficient with the added disadvantage of decreased stability. We calculate the spatial derivatives of the deformation gradient only at the particle locations similar to the meshless collocation methods.

2.2 Moving Least Square (MLS) Approximation with Taylor Series

In continuum solid mechanics, the elastic stresses inside a deformable body are computed based on the displacement vector field, which is typically defined by a deformable model with two configurations named the reference and the current configurations, respectively. The coordinates of the particles in the reference and current configurations are represented by the material $\mathbf{X} = (X, Y, Z)$ and spatial $\mathbf{x} = (x, y, z)$ coordinates respectively. The displacement vector of a particle is therefore defined as $\mathbf{u} = \begin{bmatrix} u_X & u_Y & u_Z \end{bmatrix}^T = \mathbf{x} - \mathbf{X}$.

The Green-St.Venant strain tensor is used to measure the strain

$$\varepsilon = \nabla\mathbf{u} + \nabla\mathbf{u}^T + \nabla\mathbf{u}\nabla\mathbf{u}^T\,, \tag{4}$$

where the gradient of the continuous displacement vector field $\nabla\mathbf{u}$ is essentially the derivatives of (u_x, u_y, u_z) with respect to (X, Y, Z) arranged in the Jacobian format. For an isotropic linear-elastic material, the strain ε is mapped to the stress σ by the **C** tensor that approximates the material properties and is composed of two independent coefficients, Young's Modulus and Poisson's Ratio

$$\sigma = \mathbf{C}\varepsilon\,. \tag{5}$$

We need the partial derivatives of the displacement vector field in order to compute the strain, stress, and the internal elastic forces applied to the meshless particles. Moving Least Squares (MLS) approximation is used to compute this gradient ($\nabla\mathbf{u}$).

For a central meshless particle *i* and its neighbor *j*, the value of u_x at the location of *j* can be approximated by the first order Taylor expansion as

$$\tilde{u}_{x_j} = u_{x_i} + \left.\frac{\partial u_X}{\partial \mathbf{X}}\right|_i .(\mathbf{X}_j - \mathbf{X}_i) \ . \tag{6}$$

The weighted sum of squared differences between the displacement vector and its approximation obtained from the equation (6) gives the error measure of the MLS approximation

$$e = \sum_j (\tilde{u}_{x_j} - u_{x_j})^2 w(r_{ij}) \ . \tag{7}$$

The expanded equation of the error measure for a particle *i* is therefore obtained by

$$e = \sum_j (u_{x_i} + (\frac{\partial u_x}{\partial X}) \mathrm{X}_{ij} + (\frac{\partial u_x}{\partial Y}) Y_{ij} + (\frac{\partial u_x}{\partial Z}) Z_{ij} - u_{x_j})^2 w(r_{ij}) \ . \tag{8}$$

We want to minimize this error measure for some values of $(\partial u_x)/\partial$X, $(\partial u_x)/\partial$Y, and $(\partial u_x)/\partial$Z, therefore we set the derivative of the error measure e with respect to the partial derivatives of the displacement vector to zero, resulting in three equations for three unknowns

$$\left(\sum_j (\mathbf{X}_j - \mathbf{X}_i)(\mathbf{X}_j - \mathbf{X}_i)^T w\left(r_{ij}\right) \right) \left.\frac{\partial u_x}{\partial \mathbf{X}}\right|_i = \sum_j \left(u_{x_j} - u_{x_i}\right)(\mathbf{X}_j - \mathbf{X}_i) w\left(r_{ij}\right) . \tag{9}$$

The coefficient of the partial derivative on the left-hand side of the equation (9) is the 3x3 matrix called the moment matrix (**A**). **A** can be inverted and premultiplied with both of the sides of the equation for computing the partial derivatives.

2.3 Force Calculation

The elastic body forces that are applied to the individual particles in the meshless collocation method are calculated through the strain energy density, which is a function of the particle displacements. For a particle *i* with volume v_i, strain ε_i, and stress σ_i, the strain energy density becomes

$$U_i = v_i \frac{1}{2} (\varepsilon_i \sigma_i) \ . \tag{10}$$

The elastic force per unit volume at a meshless node's location is the negative directional derivative of the above strain energy density with respect to this node's displacement. The forces applied to the particle *i* and its neighbors *j* are then

$$f_i = -\nabla_{u_{x_i}} U_i = -v_i \sigma_i \nabla_{u_{x_i}} \varepsilon_i$$
$$f_j = -\nabla_{u_{x_j}} U_i = -v_i \sigma_i \nabla_{u_{x_j}} \varepsilon_i \quad . \tag{11}$$

Eq. (11) is iterated over all particles and the total force applied to a particle is the sum of all the forces with the same index as that particle. These force components are obtained by using the Green-Saint-Venant strain tensor, which measures the linear and shear elongation. In case of a volume inverting displacement though, this strain becomes zero. In order to introduce restoring body forces in cases of volume inversion, Muller et al. [19] added another energy term to the system that penalizes deviations from a volume conserving transformation

$$U_i = \frac{1}{2} k_v (|\mathbf{J}_i| - 1)^2 \quad . \tag{12}$$

In this energy term, $\mathbf{J}_i$ is the Jacobian of the displacement vector field mapping and k_v is the volume restoration constant. Although in our experiments we have not worked on cases that cause the inversion of the volume, the effect of this term and the volume restoration constant parameter in cases of large deformations is yet to be examined.

For each of the meshless nodes, these force components are accumulated in the force vectors and then passed to the SOFA time integration module. The modular implementation of the SOFA library allows the use of different time integration schemes without changing the actual implementation of the algorithm. In this work, we used the 4th order Runge-Kutta integration scheme.

3 Implementation and Verification Techniques

In modeling and simulation studies, verification and validation of the model is a crucial step. For interactive simulations with a focus on training in particular, it is important to validate the behavior of the deformable body in order to prevent false learning outcomes. Specifically, realistic contact representation and force feedback are significant features for ensuring the validity of physically based simulators.

3.1 Meshless Method Implementation in SOFA

SOFA [12] is an open-source object-oriented software library that is targeted towards interactive medical simulations. SOFA has a modular structure that allows users to quickly prototype simulation scenes with ready-to-use components. Its object-oriented, modular architecture makes it easy for developers to extend the

functionalities of the library by deriving new components from the existing ones. The meshless elastic model described in this work has been implemented as a *force field* component, which is easily interchangeable with the existing force field components such as hexahedral finite elements or mass-spring networks. The required component interfaces such as initialization and force accumulation were implemented according to the algorithm steps described in the previous section.

Due to the nature of the presented verification method, accurate contact handling is essential to obtain precise results. Unfortunately, because of the approximating nature of the meshless methods, imposing Dirichlet boundary conditions is a challenging task on its own [24]. In this work, we have followed the approaches that were originally adopted in the SOFA library. In SOFA, constraints are filter like components, which cancel out the forces and displacements applied to their associated particles. For example for fixed node boundary conditions, SOFA's *fixed constraint* component is used to attach a meshless particle to a fixed point in the current configuration.

SOFA has support for several contact handling methods such as penalty-based and constraint-based methods. Among these, the constraint-based methods are more appealing than the former class of methods because they use Lagrange multipliers to handle complex constraints and produce physically accurate results with the additional computation cost. Lagrange multipliers with unilateral interaction laws are used to handle complex constraints. The constraints depend on the relative positions of the interacting objects, which are the meshless particles and the spherical rigid indenter in our case [12].

3.2 Contact Mechanics Theory

Hertzian theory of non-adhesive elastic contact [25] defines analytical solutions for the interaction of elastic half-spaces with simple shapes in terms of applied force and object indentation. For example, the amount of indentation of an elastic half-space under a spherical load is given by

$$F = \frac{4}{3} E^* \sqrt{R} d^{3/2}, \tag{13}$$

where F is the vertical force applied on the spherical load, R is the radius of the spherical load, d is the indentation amount, and E^* is the combined Young's modulus of the two materials and calculated using the Young's moduli (E_1, E_2) and Poisson's ratios (ν_1, ν_2) of the two materials as

$$\frac{1}{E^*} = \frac{1-\nu_1^2}{E_1} + \frac{1-\nu_2^2}{E_2}. \tag{14}$$

The Hertzian theory assumes 1) small strains within the elastic material, 2) much smaller area of contact compared to the areas of the objects in contact, and 3) continuous and frictionless contact surfaces.

The Hertzian theory is an important stepping stone in the field of contact mechanics; therefore there have been numerous finite element analysis studies about the subject that use both research and commercial finite element code [26-29].

3.3 Verification Experiments

In order to verify the usability of the Hertzian contact theory as a means of verification of soft-tissue deformation, we first conducted experiments using well-established finite element code. FEBio is an open-source software suite that is primarily targeted towards biomechanics and biophysics problems with a specific focus on nonlinear large deformation problems in biosolid mechanics [30]. FEBio provides several models and options to represent the non-adhesive Hertzian contact theory. In our experiments, we selected the facet-to-facet sliding algorithm that is based on Laursen's contact formulation [31]. In this algorithm, the contact constraints are enforced through Lagrange multipliers.

The FEBio experiment was setup by defining the fixed-position boundary conditions of the deformable block at its bottom and side faces, facet-to-facet sliding contact between the top face of the deformable block and the rigid spherical indenter, and the sphere's indentation amount. The simulation was run for 10 time steps of 0.1s each and the simulation runtime took over 4 minutes. The node at the middle of the top of the deformable block was tracked for the vertical displacement and the vertical component of the contact force. We compared the obtained load-displacement curve to the theoretical solution, which were in very good agreement (Figure 1), therefore verifying the usefulness of the Hertzian contact theory as a verification method.

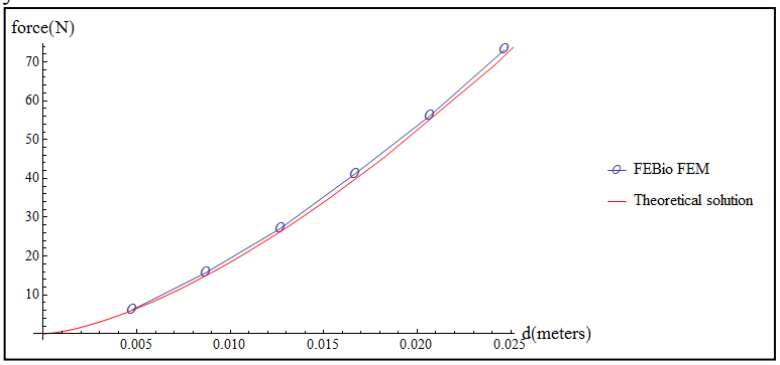

Figure 1 Comparison of the FEBio FEM Code and the theoretical solution of the Hertzian non-adhesive frictionless contact theory.

The contact mechanics experiment was setup as a SOFA scene. In order to assess the ground-truth performance of the contact handling in SOFA, the rectangular deformable block was represented with the hexahedral finite element model in addition to the described meshless method. The validation of the hexahedral FEM implementation of SOFA is studied by Marchal et al. [32]. For a given sphere radius, simulations were performed for varying force values (F) applied to the spherical load (Figure 2). With the applied force, the rigid sphere comes into contact with the block and deforms it. The vertical velocity of the sphere is monitored and the indentation of the material (d) is measured when the sphere comes to rest. This F-d pair is compared to the theoretical solution.

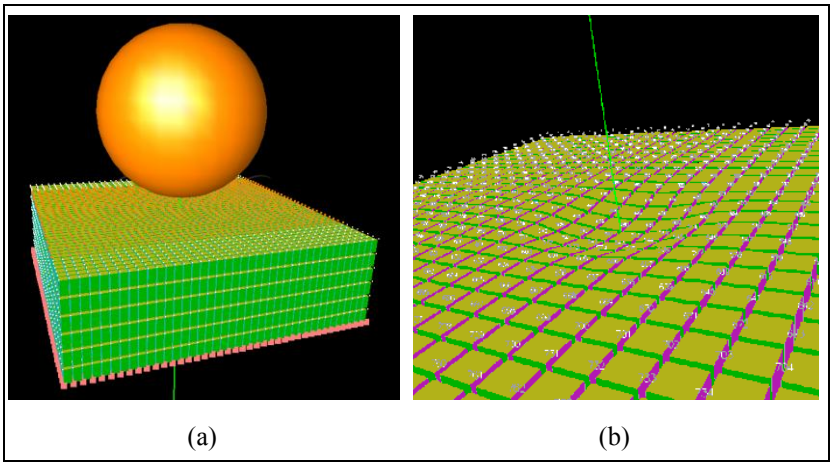

(a) (b)

Figure 2 (a) Initial setup of the indentation experiment for the SOFA FEM model, (b) the close-up view of the indented deformable material. SOFA allows the user to track and monitor simulation values of indexed particles.

The meshless nodes are distributed uniformly inside a cubical volume with 2m long edge length. The indentation experiment is repeated for several distribution configurations, which play critical role especially for the MLS approximation-based collocation methods. The convergence rate in the L2 (vector) error norm of the force-indentation pairs with respect to the theoretical values (Figure 3) is investigated. The effect of different distribution schemes on the accuracy, stability, and performance of the meshless collocation methods is yet to be examined. In our implementation, the number of neighboring nodes is limited to 16 for each of the meshless nodes.

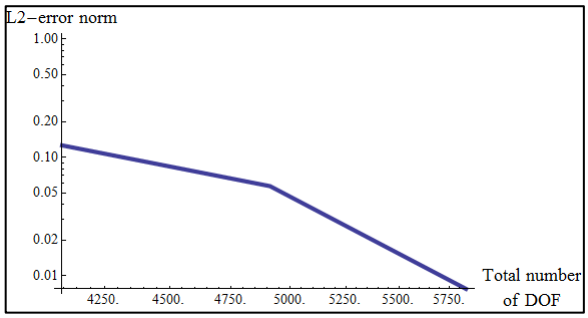

Figure 3 Error in the L2 norm with respect to the theoretical solution as functions of total number of the degrees of freedom for the (a) FEM model and (b) meshless method.

We compared the SOFA FEM implementation and the meshless collocation method with close accuracy (Figure 4). For our meshless collocation method with nodal integration, we used an explicit time integration scheme with a time step of 0.001s without any stability problem. For the SOFA FEM implementation, we had to use implicit integration with a time step of 0.01s. The calculations were performed within the SOFA application on a single Intel Core i5 CPU running at 2.67 GHz with 16 GB of RAM under Windows 7 operating system. The SOFA FEM implementation took 195ms of calculations per time step, whereas the meshless method consumed 20.11ms for calculations per time step. Therefore, the meshless collocation implementation in SOFA (along with other SOFA related operations such as collision detection) is roughly 25 times slower than the real-time operation, which is slightly better than the 30 times slower performance reported by the Meshless TLED algorithm [20]. The calculation speed of the meshless collocation algorithm is governed by the number of particles and the number of neighbors assigned to each particle.

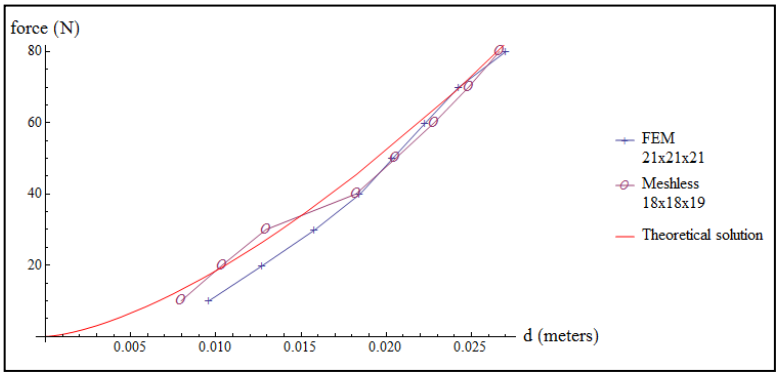

Figure 4 Comparison of the SOFA FEM implementation and the meshless collocation method with close indentation accuracy and the theoretical solution.

We also performed a mesh convergence study for the meshless collocation method by investigating the convergence of the indentation amount to the theoretical value for a fixed amount of force (Figure 5). After around 6000 particles, the indentation value converges to the theoretical indentation value.

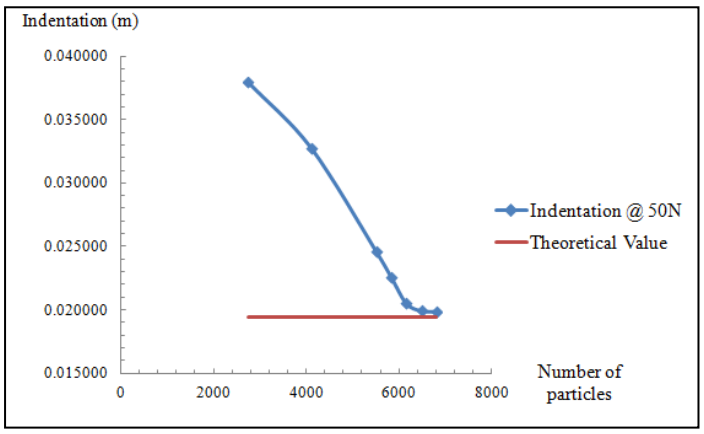

Figure 5 Convergence of the indentation value with increasing number of meshless particles.

4 Conclusions and Future Work

The discussed Moving Least Square approximation-based meshless method may be useful in continuum problems with extreme deformations or moving discontinuities such as cracks or cuts. The presented algorithm for the meshless collocation method was implemented as a component for the open source SOFA library, which is primarily targeted at real-time medical simulation. Contact mechanics-based verification experiments were conducted with FEBio FEM code, SOFA hexahedral FEM method, and the presented meshless collocation method. The convergence study results and L2 error norm curves are promising for the meshless deformable model. For the meshless collocation methods, the influence of the meshless node distribution and the size of the nodal support radii of the nodes are not well studied. The findings of our own experiments also suggest further studies of these important aspects of the meshless collocation methods.

References

[1] L. P. Nedel and D. Thalmann, "Real time muscle deformations using mass-spring systems," in *Computer Graphics International, 1998. Proceedings*, 1998, pp. 156-165.

[2] K.-J. Bathe, *Finite element procedures* vol. 2: Prentice hall Englewood Cliffs, 1996.

[3] R. Eymard*, et al.*, "Finite volume methods," *Handbook of numerical analysis,* vol. 7, pp. 713-1018, 2000.

[4] A. R. Mitchell and D. F. Griffiths, "The finite difference method in partial differential equations," *Chichester, Sussex, England and New York, Wiley-Interscience, 1980. 281 p,* 1980.

[5] T. W. Sederberg and S. R. Parry, "Free-form deformation of solid geometric models," *ACM Siggraph Computer Graphics,* vol. 20, pp. 151-160, 1986.

[6] S. F. Frisken-Gibson, "Using linked volumes to model object collisions, deformation, cutting, carving, and joining," *Visualization and Computer Graphics, IEEE Transactions on,* vol. 5, pp. 333-348, 1999.

[7] K. Waters and D. Terzopoulos, "A physical model of facial tissue and muscle articulation," in *Visualization in Biomedical Computing*, 1990, pp. 77-82.

[8] A. Van Gelder, "Approximate simulation of elastic membranes by triangulated spring meshes," *Journal of graphics tools,* vol. 3, pp. 21-42, 1998.

[9] M. Bro-Nielsen, "Finite element modeling in surgery simulation," *Proceedings of the IEEE,* vol. 86, pp. 490-503, 1998.

[10] K. Miller*, et al.*, "Total Lagrangian explicit dynamics finite element algorithm for computing soft tissue deformation," *Communications in numerical methods in engineering,* vol. 23, pp. 121-134, 2007.

[11] S. Marchesseau*, et al.*, "Multiplicative jacobian energy decomposition method for fast porous visco-hyperelastic soft tissue model," in *Medical Image Computing and Computer-Assisted Intervention–MICCAI 2010*, ed: Springer, 2010, pp. 235-242.

[12] F. Faure*, et al.*, "SOFA: a multi-model framework for interactive physical simulation," in *Soft Tissue Biomechanical Modeling for Computer Assisted Surgery*, ed: Springer, 2012, pp. 283-321.

[13] Y. Chen*, et al.*, *Meshless methods in solid mechanics*: Springer Verlag, 2006.

[14] V. P. Nguyen*, et al.*, "Meshless methods: a review and computer implementation aspects," *Mathematics and Computers in Simulation,* vol. 79, pp. 763-813, 2008.

[15] L. B. Lucy, "A numerical approach to the testing of the fission hypothesis," *The astronomical journal,* vol. 82, pp. 1013-1024, 1977.

[16] N. Sukumar. (2002, 08/01/2012). *The Natural Element Method (NEM) in Solid Mechanics*. Available: http://dilbert.engr.ucdavis.edu/~suku/nem/

[17] B. Nayroles*, et al.*, "Generalizing the finite element method: diffuse approximation and diffuse elements," *Computational mechanics,* vol. 10, pp. 307-318, 1992.

[18] T. Belytschko*, et al.*, "Element-free Galerkin methods," *International Journal for Numerical Methods in Engineering,* vol. 37, pp. 229-256, 1994.

[19] M. Müller*, et al.*, "Point based animation of elastic, plastic and melting objects," in *ACM SIGGRAPH/Eurographics symposium on Computer animation*, 2004, pp. 141-151.

[20] A. Horton*, et al.*, "A meshless total Lagrangian explicit dynamics algorithm for surgical simulation," *International Journal for Numerical Methods in Biomedical Engineering,* vol. 26, pp. 977-998, 2010.

[21] M. Pauly*, et al.*, "Meshless animation of fracturing solids," *ACM Trans. Graph.,* vol. 24, pp. 957-964, 2005.

[22] H. Si, "TetGen: A quality tetrahedral mesh generator and three-dimensional delaunay triangulator," *Weierstrass Institute for Applied Analysis and Stochastic, Berlin, Germany,* 2006.

[23] J.-D. Boissonnat*, et al.*, "Triangulations in CGAL," in *Proceedings of the sixteenth annual symposium on Computational geometry*, 2000, pp. 11-18.

[24] G.-R. Liu, *Meshfree methods: moving beyond the finite element method*: CRC press, 2010.

[25] H. Hertz, "{Über} die {B} erührung fester elastischer {K} örper," *J. für die reine u. angew. Math.,* vol. 92, 1882.

[26] D. Franke*, et al.*, "The p-version of the FEM for computational contact mechanics," *PAMM,* vol. 8, pp. 10271-10272, 2008.

[27] N. Schwarzer*, et al.*, "Comparison between analytical and FEM calculations for the contact problem of spherical indenters on layered materials," *Thin solid films,* vol. 270, pp. 279-282, 1995.

[28] D. Franke*, et al.*, "A comparison of the h-, p-, hp-, and rp-version of the FEM for the solution of the 2D Hertzian contact problem," *Computational mechanics,* vol. 45, pp. 513-522, 2010.

[29] F. Pennec*, et al.*, "Verification of contact modeling with COMSOL multiphysics software," 2007.

[30] S. A. Maas*, et al.*, "FEBio: finite elements for biomechanics," *Journal of biomechanical engineering,* vol. 134, 2012.

[31] T. Laursen and B. Maker, "An augmented Lagrangian quasi-Newton solver for constrained nonlinear finite element applications," *International Journal for Numerical Methods in Engineering,* vol. 38, pp. 3571-3590, 1995.

[32] M. Marchal*, et al.*, "Towards a framework for assessing deformable models in medical simulation," in *Biomedical Simulation*, ed: Springer, 2008, pp. 176-184.